Version of record at: https://doi.org/10.1002/aic.18033

Check for updates

Received: 28 October 2022 | Revised: 19 December 2022 | Accepted: 2 January 2023

DOI: 10.1002/aic.18033

AIChE JOURNAL

RESEARCH ARTICLE

Process Systems Engineering

# Closed-loop modeling of central and intrinsic cardiac nervous system circuits underlying cardiovascular control

Michelle M. Gee[1,2] | Abraham M. Lenhoff[1] | James S. Schwaber[1,2] | Babatunde A. Ogunnaike[1] | Rajanikanth Vadigepalli[1,2]

[1]Department of Chemical and Biomolecular Engineering, University of Delaware, Newark, Delaware, USA

[2]Daniel Baugh Institute of Functional Genomics/Computational Biology, Department of Pathology and Genomic Medicine, Thomas Jefferson University, Philadelphia, Pennsylvania, USA

**Correspondence**
Rajanikanth Vadigepalli, Daniel Baugh Institute of Functional Genomics/Computational Biology, Department of Pathology and Genomic Medicine, Thomas Jefferson University, Philadelphia, PA 19107, USA.
Email: rajanikanth.vadigepalli@jefferson.edu

**Funding information**
National Heart, Lung, and Blood Institute, Grant/Award Numbers: R01 HL161696, U01 HL133360; National Science Foundation, Grant/Award Numbers: 1940700, OAC-1919839; NIH Office of the Director, Grant/Award Number: OT2 OD030534

## Abstract

The baroreflex is a multi-input, multi-output physiological control system that regulates blood pressure by modulating nerve activity between the brainstem and the heart. Existing computational models of the baroreflex do not explicitly incorporate the intrinsic cardiac nervous system (ICN), which mediates central control of heart function. We developed a computational model of closed-loop cardiovascular control by integrating a network representation of the ICN within central control reflex circuits. We examined central and local contributions to the control of heart rate, ventricular functions, and respiratory sinus arrhythmia (RSA). Our simulations match the experimentally observed relationship between RSA and lung tidal volume. Our simulations predicted the relative contributions of the sensory and the motor neuron pathways to the experimentally observed changes in the heart rate. Our closed-loop cardiovascular control model is primed for evaluating bioelectronic interventions to treat heart failure and renormalize cardiovascular physiology.

**KEYWORDS**
baroreceptor reflex, estimation and control in biological systems, intrinsic cardiac nervous system, physiological modeling, vagus nerve stimulation

## 1 | INTRODUCTION

The cardiovascular system ensures adequate blood supply to the entire body and requires the coordination of several organs through a complex system of signals that are mediated by the nervous system. The primary objective of cardiovascular homeostasis is to maintain near-constant blood pressure while balancing multiple demands for blood flow to different organs, including coping with disturbances such as those caused by respiration or exercise. This objective is carried out on a beat-to-beat basis by the baroreceptor reflex—a nonlinear control system that modulates the involuntary parasympathetic and sympathetic nerve activity between the brainstem and the heart (Figure 1). Parasympathetic (vagal) and sympathetic nerve activity exert opposing effects of decreasing and increasing heart rate, respectively, and an imbalance in parasympathetic and sympathetic nerve activity has been associated with cardiovascular disease.[1–5] In addition to the brainstem and spinal cord-driven central cardiovascular control, there exists an extensive neural circuit within the heart,

This work is in memory of Dr. Babatunde A. Ogunnaike, who co-advised Michelle M. Gee and guided the model development and analysis, and represents a milestone in the 30-year collaboration between Dr. Ogunnaike and Drs. Schwaber and Vadigepalli.

This is an open access article under the terms of the Creative Commons Attribution-NonCommercial-NoDerivs License, which permits use and distribution in any medium, provided the original work is properly cited, the use is non-commercial and no modifications or adaptations are made.
© 2023 The Authors. *AIChE Journal* published by Wiley Periodicals LLC on behalf of American Institute of Chemical Engineers.

Version of record at: https://doi.org/10.1002/aic.18033



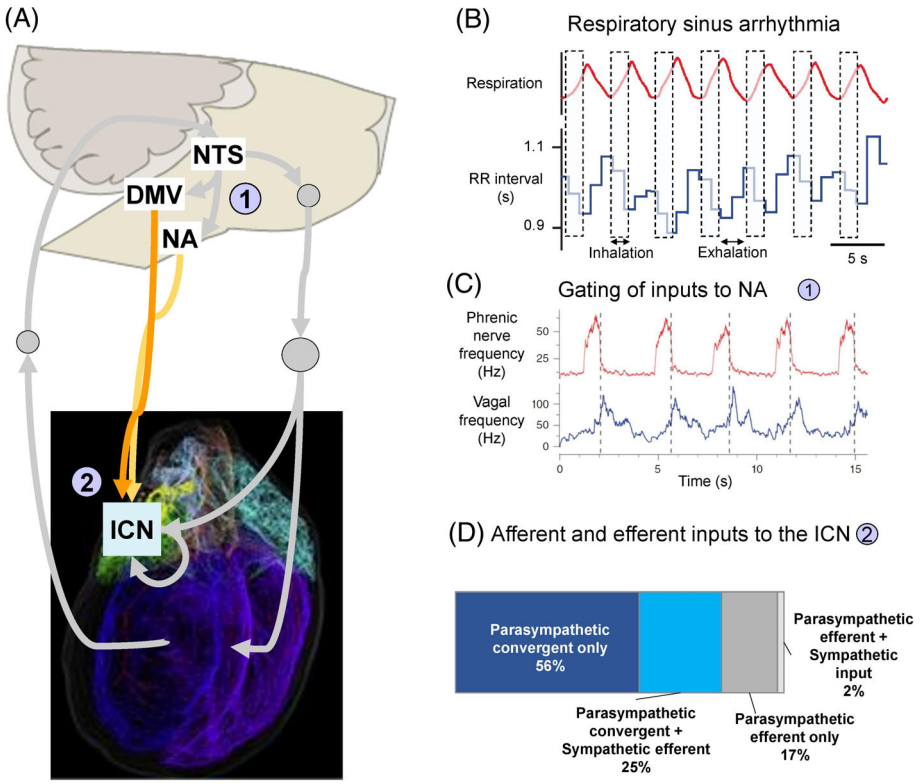


**FIGURE 1** Translation of the baroreceptor reflex to a control system representation including central (brainstem) and local (ICN) contributions to RSA based on anatomical and physiological evidence. (A) Anatomical representation of neural control of the heart highlighting (1) gating of inputs to the nucleus ambiguus (NA) hypothesized to contribute to respiratory sinus arrhythmia (RSA) and (2) the ICN as the controller for an inner control loop that integrates sensory information. Heart image adapted from Achanta et al.[6] (B) Representative RSA behavior showing RR interval (reciprocal of heart rate) synchronization with ventilation. RR interval decreases during inhalation and decreases during exhalation.[7] (C) Central contributions to RSA. Vagal nerve activity transmitted from the brain to the heart oscillates with respiratory signals from the phrenic nerve, which is an indicator of respiratory activity. Image adapted from Farmer et al.[8] (D) The ICN facilitates the local cardiac reflex with evidence that ~75% of ICN neurons are convergent with inputs from both afferent (sensory) and efferent (from the brainstem) inputs.[9] DMV, dorsal motor nucleus of the vagus; ICN, intrinsic cardiac nervous system; NA, nucleus ambiguus; NTS, nucleus tractus solitarius.

termed the intrinsic cardiac nervous system (ICN), which mediates the central control of heart functions.[10–12] The ICN is responsible for the integration of the parasympathetic and sympathetic outflow from the brainstem and local sensory feedback.[9,13] Recent efforts by the Cardiac Consortium of the National Institutes of Health (NIH) Common Fund Stimulating Peripheral Activity to Relieve Conditions (SPARC) program have delineated extensively the anatomical, connectional, molecular, and physiological aspects of the ICN.[6,14,15]

Although the baroreflex and its contributions to cardiovascular physiology have been studied extensively using computational models,[3,16–20] these models do not account explicitly for the ICN. An earlier study by several of the present authors has focused on modeling the cardiac local reflex using computational neuroscience-based approaches for detailed representations of the ion channel physiology and the biochemistry of signaling pathways.[21] However, this model did not incorporate the brainstem neural circuits. Single-cell gene expression studies have led to a delineation of the neuronal cell states and subtypes in the brainstem autonomic control circuits that mediate the baroreflex, providing new information to update the models of closed-loop cardiovascular control.[22] A computational model-based study from our group has built on these experimental studies to develop a transfer function-based representation of the closed-loop cardiovascular control circuit that delineated the neuronal subtypes within the brainstem.[3] This model was used to examine the effect of adaptation in brainstem neurons on the changes in cardiovascular physiology and baroreflex control following exercise as well as heart failure.

Recent studies have highlighted the role of interaction between respiration and heart health through respiratory sinus arrhythmia (RSA), which is a natural heart rate increase during inhalation and decrease in heart rate during exhalation that is decreased during cardiovascular disease states, including heart failure. The restoration of RSA using a pacemaker has been found to increase stroke volume and cardiac output in rat models of heart failure compared with pacemakers that do not mimic RSA, indicating that RSA is a cause rather than an effect of cardiovascular health.[23] Similar findings of increased cardiac output with the restoration of RSA were found for sheep with pacemakers to treat heart failure with reduced ejection fraction.[24]

The beneficial potential of restoring RSA during cardiovascular disease is not limited to cardiac pacemakers. Vagal nerve stimulation (VNS) is an emerging bioelectronic treatment for heart failure[25–28] and cardiac arrhythmias[4,29] and is one therapy that could leverage these findings on the beneficial effects of the restoration of RSA. VNS involves stimulation of the vagus nerve, which connects the brain and the heart, with an electrical current using an external electronic device that could be used to restore RSA. Therefore, modeling the central and local autonomic influences on cardiorespiratory interactions could

Version of record at: https://doi.org/10.1002/aic.18033



**TABLE 1** Summary of experimental data sources for model development

| Reference | Cardiovascular function studied | Experimental model | | Number of replicates used in study | Perturbation (inputs) | Relevant measure (outputs) used in model development |
|---|---|---|---|---|---|---|
| Iano et al.[30] | HR (in response to vagal activity timing) | Canine | | 7 | Cervical vagus trunk stimulation | HR |
| Falkenburger et al.[31] | Muscarinic receptor activation time | In vitro human kidney cells | | >10,000 cells/ sample | N/A | Muscarinic receptor activation time delay |
| Rajendran et al.[15] | ICN firing frequency, HR | Pig | | 1 pig, 7 neurons | Cervical vagus trunk stimulation | ICN neuron firing frequency, HR |
| Yamakawa et al.[32] | HR, SBP, DBP | Pig | | 12 | Cervical vagus trunk stimulation | HR, SBP, DBP |
| Kobayashi[33] | Respiratory sinus arrhythmia amplitude | Human | Men (ages 21–24) | 8 | Lung tidal volume | Respiratory sinus arrhythmia amplitude |
| Teixeira et al.[34] | HR in women | Human | Women (ages 18–35) | 44 | None | HR |
| Cain et al.[35] | Cardiovascular outputs of healthy patients across age groups | Human | Youths and adults | 20 (children), 76 (adults) | None—echo cardiac magnetic imaging | CO, EF, SBP, DBP |

Abbreviations: CO, cardiac output; DBP, diastolic blood pressure; EF, ejection fraction; HR, heart rate; ICN, intrinsic cardiac nervous system; SBP, systolic blood pressure.

be utilized to develop therapeutic targets in the treatment of heart failure.

Here, we built on the prior modeling studies to develop a computational model of closed-loop cardiovascular control that explicitly incorporates the ICN and its interaction with the local sensory feedback within the heart as well as the brainstem-mediated central control circuits. In addition, our model accounts for the effects of RSA on cardiac physiology and closed-loop control. The inclusion of autonomic regulation allowed us to probe the role of the ICN in local cardiovascular control and RSA in the extended model. We tuned the model parameters to experimental data on heart rate, elastance, and ICN activity and compared the model predictions with the experimental data relating the lung tidal volume and the amplitude of RSA. We then used the model to predict the effects of VNS under multiple scenarios representing differential recruitment and stimulation of sensory and motor neurons. Our model predictions provide new insights into the experimental data on VNS by predicting the balance of sensory versus motor neuron stimulation that is likely to underlie the in vivo observations.

## 2 | METHODS

We build upon prior models[3,16,36–39] by including additional model components based on recently collected data to represent more precisely the ICN and its regulation of cardiovascular functions and RSA.[6,14] A summary of the experimental data used to estimate model parameters is included in Table 1.

### 2.1 | Extended model structure

The present model was extended from prior models to include (1) a representation of the gating of inputs to the nucleus ambiguus (NA), which is the brainstem structure that contributes to heart rate control, and (2) a representation of the ICN (Figures 1A and 2). These structures represent central (NA) and local (ICN) contributions to RSA. All model equations that were added to the extended model and the original model equations are included in Supporting Information.[3] The addition of the ICN to the model enables representations of both central (brainstem) and local (sensory) contributions to cardiovascular dynamics. To represent the local contributions, we included the ICN, which incorporates sensory information in an inner feedback loop, and updated the effector function that represents the effect of vagal activity on the heart to account for the addition of the ICN to the model (Figures 1A and 2). To represent central contributions to RSA, we added a gate to modulate the inputs to the NA as described by physiological experiments[40–44] and other computational models[45] (Figures 1A and 2).

### 2.2 | Central contributions to RSA and outflow of the sympathetic and parasympathetic nervous systems

The extended model builds on the functions developed by Park et al.[3] to represent the outflow from the nucleus tractus solitarius (NTS) to the NA and dorsal motor nucleus of the vagus (DMV) (see Figure 1 caption

Version of record at: https://doi.org/10.1002/aic.18033



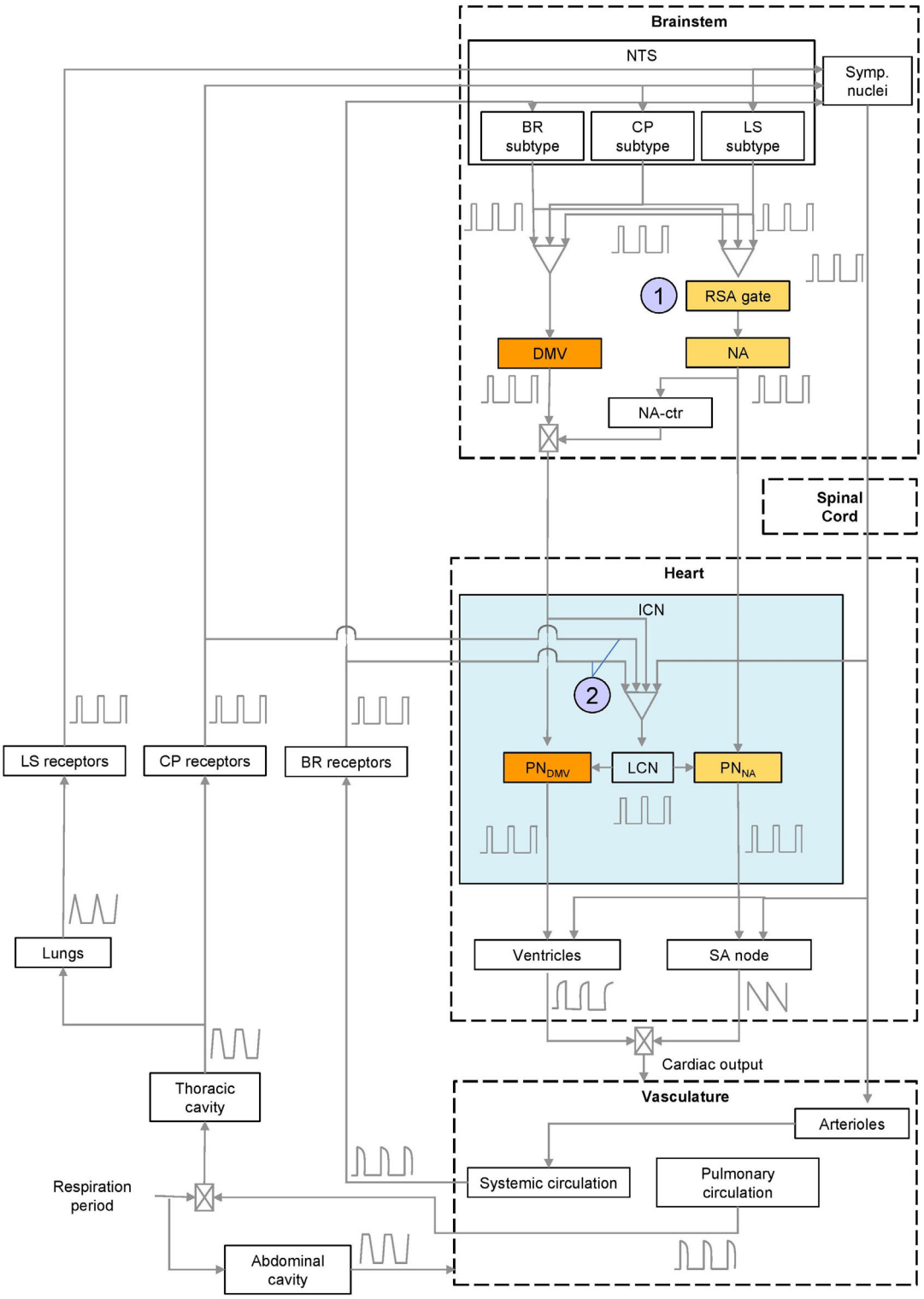


**FIGURE 2** The control block diagram of the cardiovascular system and neural control components incorporated in a closed-loop model, which includes (1) gating of inputs to the nucleus ambiguus (NA) based on the respiratory phase and (2) the intrinsic cardiac nervous system (ICN) which includes the local reflex that provides sensory information. The model contains three types of sensors: baroreceptors (BR) that sense blood pressure changes in the arteries, cardiopulmonary receptors (CPR) that sense blood pressure changes in the atria and ventricles, and lung stretch receptors (LSR) that sense lung inflation. These sensory inputs are integrated in the nucleus tractus solitarius (NTS), a neuronal group in the brainstem that integrates sensory input. The NTS has three subgroups representing separate neuronal subtypes with different afferent input types corresponding to the three receptor types. The NTS projects to the NA and the dorsal motor nucleus of the vagus (DMV), the two primary lanes of vagal outflow to the heart. The activation of NA is gated based on the phase of the respiratory cycle to account for respiratory sinus arrhythmia (RSA). The two lanes innervate the ICN and target separate populations of principal neurons (PN), which receive direct input from the brainstem. PNs also receive input from local circuit neurons (LCN), which integrate local cardiac afferent feedback and sympathetic input. ICN activity controls the sinoatrial (SA) node and ventricles which contribute to heart rate and blood pressure, respectively in the cardiovascular system model. Details of parameters and equations are included in Data S1. NA-ctr, nucleus ambiguus activity affecting ventricular elastance (a surrogate for contractility); Symp., sympathetic.

Version of record at: https://doi.org/10.1002/aic.18033



for an explanation of neuron groups). Physiological evidence indicates that the gating of inputs to the NA could cause RSA.[40–44] Thus, an additional gating function to modulate the outputs of the NTS that go to the NA ($ff_{NA,input}$) based on the phase of the respiratory cycle was added to the extended model to capture RSA (Figure 2).

$$ff_{NA,input} = \begin{cases} K_{RSA} * ff_{NTS,output}, & s < \dfrac{T_{insp}}{T_{resp}} \\ ff_{NTS,output}, & s \geq \dfrac{T_{insp}}{T_{resp}} \end{cases}. \quad (1)$$

The respiratory phase, $s$, varies between zero and one and resets to zero at the end of each respiratory cycle. The inspiration and postinhalation phases of $s$ are defined using the inhalation time ($T_{insp}$) divided by the total respiratory cycle time ($T_{resp}$). Outputs from the NTS ($ff_{NTS,output}$) are decreased by a gain value ($K_{RSA}$) during inspiration but are unaffected during exhalation to mimic the observed NA input gating behavior.

## 2.3 | ICN contributions to neural input to the heart

As the final point of cardiac nervous control, the ICN is an important addition to the model that mediates the local cardiac reflex and integrates parasympathetic, sympathetic, and sensory information via principal neurons and local circuit neurons (LCNs).[46,47] Experimental evidence indicates that there are two distinct lanes of vagal input from the brainstem to the ICN, one from the NA and one from the DMV.[11,48,49] Physiological experiments indicate that the NA is responsible primarily for controlling heart rate, while the DMV contributes to contractility.[50–54] These vagal inputs target separate populations of principal neurons in the ICN: principal neurons that receive input from the NA ($PN_{NA}$) and principal neurons that receive input from the DMV ($PN_{DMV}$).[11,48,51] Because the principal neurons that receive their inputs from the DMV transmit their signal via muscarinic receptors, which have a modulatory response extending over approximately 7 s, we also include a first-order filter with time delay for this neuronal population.[31,50,52] The output, filtered ($ff_{filtered,PNDMV}$) is delayed by $\tau_{PNDMV}$ compared to the input ($ff_{out,PNDMV}$).

$$\frac{dff_{filtered,PN_{DMV}}}{dt} = \tau_{PN_{DMV}}\left(ff_{out,PN_{DMV}} - ff_{filtered,PN_{DMV}}\right). \quad (2)$$

Both principal neuron populations also receive inputs from LCNs embedded in the ICN, which integrate inputs from the DMV, sympathetic activity, and local sensory activity.[9,10,55] Sensory afferents are popular clinical targets for cardiovascular diseases, and in our model, sensory inputs to the LCNs constitute an inner feedback loop, which contributes to cardiovascular control.[56–58] Consequently, the principal neuron populations and LCNs represent key targets for continued investigation of regulation of cardiac function and contribution to RSA. Thus, to extend prior models to reflect more accurately the physiological components regulating parasympathetic activity and possible RSA mechanisms, we included additional model components

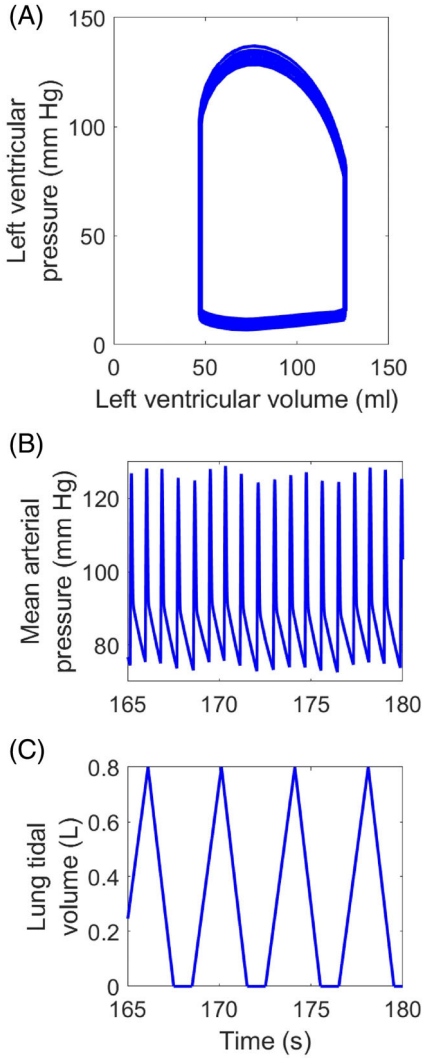


**FIGURE 3** Closed-loop model behavior at steady-state. (A) Left ventricular pressure-volume loop. (B) Mean arterial pressure and (C) lung tidal volume.

that represent principal neurons that receive direct inputs from the NA, principal neurons that receive direct inputs from the DMV, and LCNs that integrate sensory inputs in an inner feedback loop.[3] Each of these neuronal populations is represented by a sigmoidal function to capture the saturating firing behavior of neurons, which is a well-known characteristic of the baroreflex.[16,59,60]

$$f_{out,j} = \frac{f_{min,j} - f_{max,j}}{1 + \left(\frac{f_{input,j}}{f_{midpt,j}}\right)^{k}} + f_{max,j}. \quad (3)$$

The parameters describe the maximum ($f_{max}$) and minimum ($f_{min}$) output firing frequency of the jth neuronal group, the input firing frequency to which the neuronal group is most sensitive ($f_{midpt}$), and the gain ($k$) describing the rate of change in output firing frequency given a change in input firing frequency. This equation was updated from Park et al.[3] so that the same sigmoid was used, but the representation of the gain parameter was modified so it is proportional to the output firing rate.

Version of record at: https://doi.org/10.1002/aic.18033



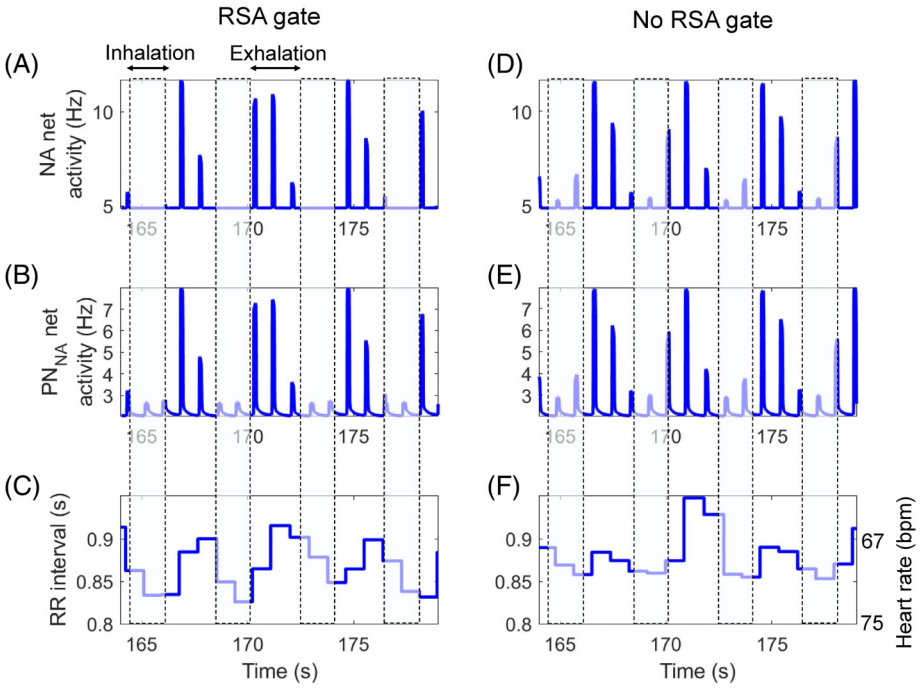


**FIGURE 4** Comparison of closed-loop model behavior with and without an RSA gate. Firing frequencies for brainstem and ICN neuronal groups regulating RR interval and the resulting RR interval are shown. (A–C) Behavior of model with gating of inputs to the NA. Activity of the NA decreases during inhalation and that decreased activity propagates to the principal neurons in the ICN that regulate RR interval. The resulting RR interval is depressed during inhalation, as is characteristic of RSA. (D–F) Behavior of model without gating of inputs to the NA. Activity of the NA decreases during inhalation due to feedback from the baroreceptors and cardiopulmonary receptors, but it is not consistent or pronounced. As a result, the activity of the PNs in the ICN also varies inconsistently with respiration. ICN, intrinsic cardiac nervous system; RSA, respiratory sinus arrhythmia; NA, nucleus ambiguus; PNs, principal neurons; $PN_{NA}$, principal neurons with inputs from the NA.

## 2.4 | Autonomic regulation of effector functions—heart rate and ventricular elastance

In prior models and the extended model, an increase in the firing frequency of an afferent input results in a reduction in the firing frequency of sympathetic nerves and a simultaneous increase in vagal nerve activity.[3] Effector functions translate the decrease in sympathetic activity and increase in vagal activity to a decrease in heart rate.

The extended model modifies the effector functions developed by Ursino and Magosso[37] and used by Park et al.[3] to represent the relationship between afferent inputs relaying peripheral sensory information and sympathetic and parasympathetic efferent outflow because of the addition of the ICN in the extended model. The inclusion of principal neurons means that the timing of vagal stimulation relative to the phase of the cardiac cycle becomes important.[21] Physiological evidence indicates that vagal nerve activity occurring near the beginning of the cardiac cycle causes larger decreases in heart rate compared with vagal nerve activity occurring near the end of the cardiac cycle.[30,61] To model this phenomenon, experimental data from dogs on the percent change in heart rate as a function of the time of vagal activity since the start of the cardiac cycle were used to calculate the percent change of the calculated heart rate.[30]

## 2.5 | Parameter estimation

Completing the model formulation required determining values for model parameters that would produce simulation results matching observed physiological behavior. For the parts of the model that were based on a prior model, we used the same parameter values as those in the original model.[3] Because the form of the sigmoidal equations used to describe brainstem neuronal groups was updated in the current model to express the gain more cleanly, parameter values for brainstem neuronal groups were updated to reproduce behavior from the prior model.[3] The remaining parameter values were selected to produce simulations that best matched experimental data associated with healthy conditions and electrophysiological behavior or were estimated from experimental data when more precise information from experiments relevant to vagal activity timing[30] and muscarinic receptor time delay[31] was available. Because we combined data from multiple sources and of different types, we have summarized key experimental details, including the model type used, number of replicates, and measured outputs for reference (Table 1). A global parametric sensitivity analysis using the PAWN method was performed to test the model robustness and is included in Figure S1.[62]

## 2.6 | ICN parameter estimation

Given that the model is highly nonlinear and the available experimental data are measurements of overall cardiac function and electrophysiological behavior in response to a stimulus, the use of multiple sigmoidal functions to represent the dynamic behavior of ICN subpopulations raises the possibility of over-parametrization. Therefore, several distinct sets of parameter values could produce similar predicted cardiovascular system behaviors. Indeed, previous experiments analyzing transcriptomic profiles of single neurons have shown that ICN and other neurons exist in multiple functional states that may be

Version of record at: https://doi.org/10.1002/aic.18033



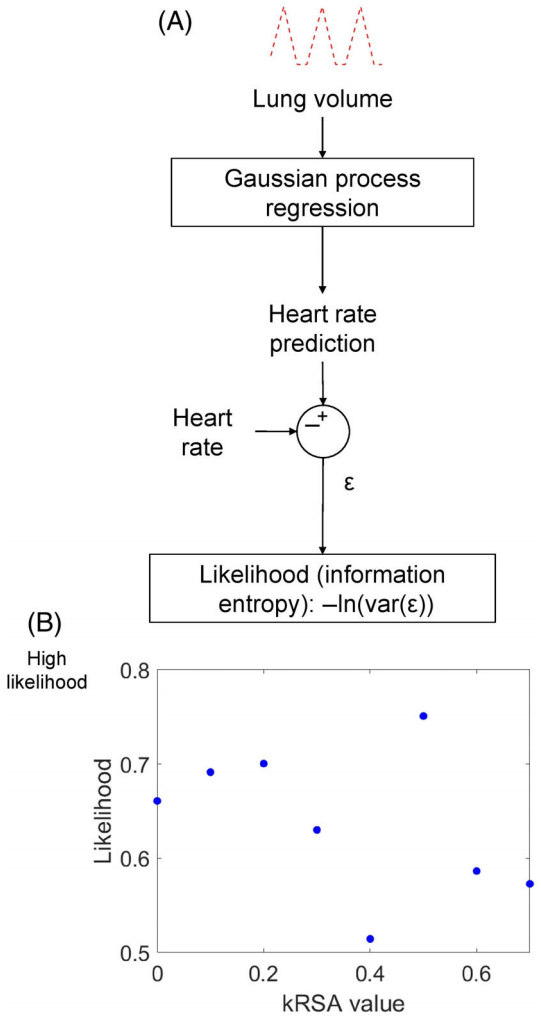


**FIGURE 5** Quantification of respiratory sinus arrhythmia behavior using Gaussian process regression to determine the likelihood that the variation in respiration is causing the variation in heart rate that is characteristic of respiratory sinus arrhythmia (RSA). (A) Workflow to determine likelihood that changes in respiration cause changes in heart rate using Gaussian process regression to predict the heart rate. The error is calculated as the difference between the predicted and actual heart rate. Likelihood is calculated from −ln(var(ε)), which quantifies the information entropy transferred from one signal to the other. (C) RSA gain (kRSA) was selected based on the value that gave the highest likelihood and still produced a significant decrease in net activity in the nucleus ambiguus (NA) during inspiration.

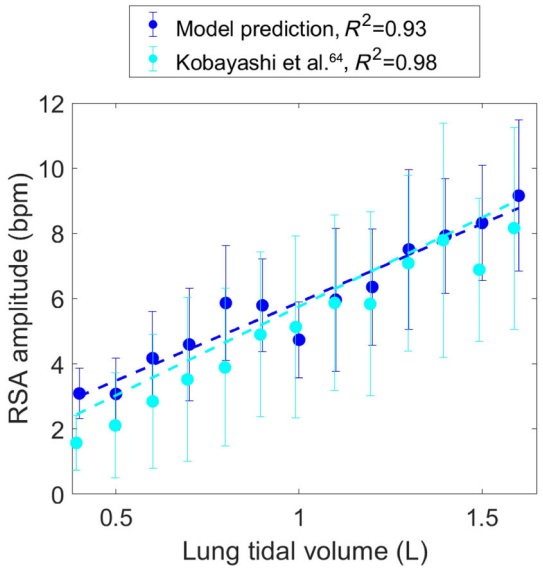


**FIGURE 6** Comparison of emergent respiratory sinus arrhythmia (RSA) behavior for the closed-loop model at different lung tidal volumes (blue) to experimental data (cyan) in humans.[33] The RSA amplitude was calculated as the difference between the minimum and the maximum heart rate over a 5-s period.[33] Respiratory rates of 0.25 Hz were used in the model and for the experimental data collection. Error bars show standard deviations. For the model, samples were collected over multiple time frames and averaged. For the experimental data, samples were collected from multiple subjects and averaged.

described by these distinct sets of parameter values.[3,14] Thus, we identified sets of parameter values that describe plausible functional states of ICN neurons.

We adapted the method used by Park et al.[3] to address the issue of non-uniqueness. Briefly, we constrained the possible parameter space to ensure that estimated firing frequencies of ICN neurons were comparable to reported values and to a ±5-fold range of similar parameters for neuronal subtypes.[15] Due to the limited data available and the possibility of nonlinear interactions between parameter values, we used a Sobol sampling approach to select 5000 sample sets.[3,63–65] We simulated a 1 Hz step input to the vagus for 1 min, then removed the step input for 1 min to match the experimental setup,[15] and calculated the average heart rate and ICN firing frequency before, during, and after VNS. We then selected the 10 sets of parameter values with the lowest mean square error when calculated with mean ICN firing frequency, mean heart rate, and mean elastance, to further constrain the sample space for a second round of Sobol sampling with 5000 sets of parameter values. The overall maximum and minimum values for each parameter from the 10 parameter sets were used as the new bounds for the second round of Sobol sampling. Target ICN neuron firing frequencies were based on experimental electrophysiology data from seven ICN neurons from an anesthetized male Yorkshire pig.[15] Because the pig had been treated with anesthesia, which can suppress heart rate responses to blood pressure changes,[66] and the model predicts human cardiovascular dynamics, the baseline heart rate, and elastance were based on a prior model.[3]

## 2.7 | RSA parameter estimation

We assessed each model's ability to produce RSA using a causal analysis between lung volume and heart rate.[67,68] Assuming that variations in the lung volume cause variations in the heart rate, a Gaussian process regression model (MATLAB R2020b) was used to predict the heart rate given the lung volume. The Gaussian process regression model was chosen because it is well suited to handle the stochastic component of the heart rate signal, and a parametric relationship between lung tidal volume and heart rate was unknown.

Version of record at: https://doi.org/10.1002/aic.18033



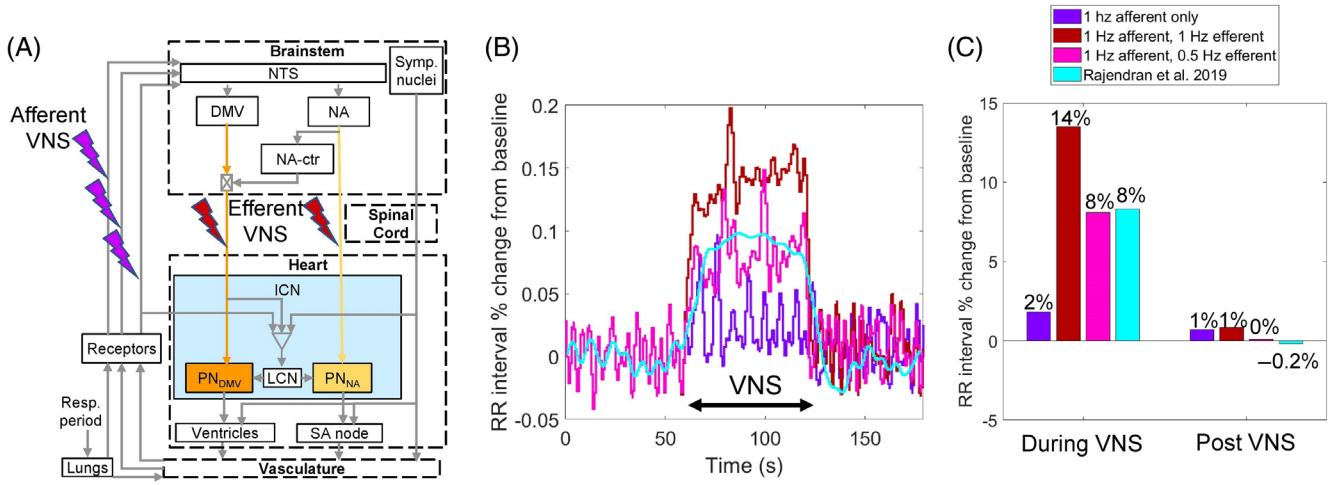


**FIGURE 7** Model tuning to heart rate and ICN activity in response to a 1 Hz VNS step input. (A) Schematic of the simulation of cervical VNS based on the experimental setup.[15] Both efferents and afferents were stimulated given that the vagus is a mixed nerve fiber and selective stimulation was not performed experimentally. While not shown in the schematic, the RSA gate is present in the model. (B) Simulated and experimental percent change in RR interval in response to cervical VNS for 1 min. Experimental VNS was performed at 1 Hz (cyan). Simulated VNS was performed at 1 Hz for afferents only (purple), 1 Hz for efferents and afferents (red), and 1 Hz for afferents with 0.5 Hz for efferents (pink). Experimental data were collected in Yorkshire pigs, which are observed to have lower RSA amplitudes than humans.[69] For ease of visualization, all RR interval signals were passed through a low pass filter (MATLAB lowpass function) with a normalized bandpass frequency of 0.15. (C) Comparison of average heart rate percent change from baseline heart rate for the model and experimental data. The baseline heart rate was averaged over the minute preceding the start of VNS. DMV, dorsal motor nucleus of the vagus; ICN, intrinsic cardiac nervous system; LCN, local circuit neuron; NA, nucleus ambiguus; NA-ctr, nucleus ambiguus affecting ventricular elastance (a surrogate for contractility); NTS, nucleus tractus solitarius; PN, principal neuron; SA, sinoatrial; VNS, vagal nerve stimulation.

We then used likelihood ($L$) as a metric to quantify how well changes in the lung volume predicted changes in the heart rate using the information entropy and compared it across RSA gate gain values.[67,68]

$$L = -\ln(\mathrm{var}(y - y_{\mathrm{pred}})). \tag{4}$$

The likelihood was calculated based on the variance of the difference between the heart rate ($y$) and the heart rate predicted ($y_{\mathrm{pred}}$) by Gaussian process regression using the lung tidal volume as the input.

## 2.8 | Simulation platform and model reproducibility

We developed the extended model on the SIMULINK (MathWorks) platform because of its suitability for modeling control systems. The ordinary differential equations in the blocks are solved using ODE15s with a $10^{-3}$ error tolerance.[3] For parameter estimation and sensitivity analysis, a high-performance computing platform was used to run the simulations on SIMULINK in parallel.

For the purpose of following best practices for credible modeling, all model files were downloaded from GitHub (https://github.com/Daniel-Baugh-Institute/CardiovascularControl/tree/main/v03; Version 3, 2022), and all simulation results and figures presented in this work were replicated independently by a research group member not involved in the original modeling and simulation study. Parameter values in the code were cross-checked for consistency against the values provided in Supporting Information. Self-assessment of the Ten Simple Rules for Credible Practice in Modeling and Simulation in Healthcare was performed and is included in the Supporting Information.[70]

# 3 | RESULTS AND DISCUSSION

## 3.1 | Closed-loop model behavior

The model's closed-loop, steady-state behavior demonstrates its ability to reproduce the qualitative characteristics of cardiovascular behavior. The left ventricular pressure–volume loop matches the experimentally observed forms (Figure 3A). The model predictions of arterial pressure (Figure 3B) and lung tidal volume (Figure 3C), two of the types of feedback that our model responds to, are shown. The arterial pressure oscillates on a beat-to-beat basis, while the lung tidal volume generally oscillates on a slower cycle depending on respiratory frequency.

## 3.2 | Model exhibits a linear relationship between lung tidal volume and RSA amplitude

Gating the inputs to the NA based on respiration introduces RSA behavior to the model. When the gate is present, NA activity is decreased during inspiration (Figure 4A). As a result, the principal neurons that receive inputs from the NA also have intermittent activity that is synchronized with respiration, which leads to RR interval

Version of record at: https://doi.org/10.1002/aic.18033



**TABLE 2** Closed-loop model predictions of cardiovascular metrics compared to reported values and standard deviations in healthy women.[34,35] Comparison of percent change in cardiovascular metrics before and during left cervical vagal nerve stimulation. The stimulation frequency of 3.5 Hz to the afferents and 1.75 Hz to the efferents was chosen to match the percent heart rate change from the experiment in Yorkshire pigs.[32] Analogously, in the experiment, stimulation intensity was chosen to achieve an approximately 10% change in heart rate from baseline to stimulation.

| | Baseline | | % change during VNS | |
|---|---|---|---|---|
| Parameter | Model predictions | Experimental mean ± SD[34,35] | Model prediction | Experimental[32] |
| Systolic pressure (mm Hg) | 126 | 123 ± 11 | −9 | −7 |
| Diastolic pressure (mm Hg) | 74 | 72 ± 8 | −14 | −11 |
| Heart rate (bpm) | 69 | 68 ± 8 | −12 | −13 |
| Cardiac output (ml/s) | 92 | 85 ± 21 | −9 | Not reported |
| Ejection fraction (−) | 0.62 | 0.64 ± 0.08 | 0 | Not reported |

(reciprocal of heart rate) decreases in synchronization with respiration (Figure 4B,C). Without the RSA gate, activity in the NA is variable, which leads to variability in activity in the principal neurons that receive inputs from the NA and an RR interval that does not decrease consistently during inhalation (Figure 4D–F).

To tune the gain value for the attenuation of input activity to the NA during inhalation, Gaussian process regression was used to select the value that produced behaviors that best captured RSA because it was difficult visually to distinguish model behavior that captured RSA (Figure 5A). A parameter sweep of gain values representing the degree of attenuation of the input signal to the NA was performed and the value that produced the highest likelihood was selected (Figure 5B).

To validate our implementation of RSA, we simulated RSA amplitude changes in response to changing lung tidal volume and compared the results with experimental data (Figure 6).[33] The RSA amplitude is the difference between the maximum and the minimum heart rate for a given time period and is independent of the synchronization with respiration that was quantified using the information entropy metric likelihood. Both the slope and the amplitude predicted by the present model agree with experimental results,[33] indicating that the model is able to capture RSA behavior over a variety of lung tidal volumes. In addition, the RSA amplitude calculated by the model increases approximately linearly with increasing lung tidal volume ($R^2 = 0.93$), consistent with experimental observations.[33] These results are due to the mechanistic nature of the model and the qualitative trend can be understood intuitively in that a larger breath volume will engage the lung stretch receptors over a wider range, which will increase the range of afferent inputs to the NTS. The range of the afferent outflow to the heart will also be larger, resulting in an increased RSA amplitude. Thus, the agreement between the model predictions and the experimental data on the relationship between lung tidal volume and RSA amplitude indicates that the model captures some of the dynamics of the cardiorespiratory system.[33]

The trends in RSA amplitude also display a degree of stochasticity that is unexpected in a deterministic model such as ours. Typically, cardiorespiratory models exhibit phase locking of cardiovascular oscillations (beat-to-beat blood pressure changes) and slower respiratory oscillations, which causes the heart rate to oscillate in a repetitive pattern.[3,71] Previously, our group had shown that the local reflex contributes to the disruption of cardiorespiratory phase locking, which attenuates the nonlinearity of the cardiac vagal drive and arterial pressure relationship.[21] The current model, which was constructed from an independent framework, supports the notion that the local reflex plays a role in disrupting cardiorespiratory phase locking.

### 3.3 | Differential activation of vagal efferents and afferents in VNS modeling

As previously described, the ICN parameters were selected using ICN neuronal activity and heart rate data in response to cervical VNS.[15] The simulated RR interval response to cervical VNS was higher than the observed RR interval change from experiments (Figure 7B). However, the vagus nerve is mixed, with approximately 20% efferents from the brain and 80% sensory afferents transmitting signals to the brain (Figure 7A).[72] Thus, we hypothesized that stimulation is delivered disproportionately to the sensory afferents and we were unable to simulate the experimental data because we were representing VNS as an equal stimulus to both efferents and afferents.[15] To test this hypothesis, we simulated additionally VNS in which (1) only the afferents were stimulated at 1 Hz and (2) the afferents were stimulated at 1 Hz and the efferents were stimulated at 0.5 Hz. The increase in the RR interval during VNS when only the afferents were stimulated was only 2% given that the brainstem modulates the signal from the afferents before sending it to the heart. When the afferents were stimulated at 1 Hz and the efferents were stimulated at 0.5 Hz, the RR interval increased by 8% during VNS and 0.1% after VNS, matching experimental results. Although afferent fibers comprise the majority of the vagus nerve fiber, our results indicate that stimulation of the efferents has a larger effect on cardiovascular behavior.

The differential activation of vagal efferents and afferents may be due to several complexities of neuron activation in VNS. Experimentally, different stimulation parameters are known to activate different diameter nerve fibers preferentially, in which larger diameter A-fibers activate at lower stimulation intensities than medium diameter B-fibers and small diameter C-fibers.[73,74] Given that A-fibers mainly are vagal afferents, they may have been activated preferentially.[75] Thus, the same stimulus may activate afferents preferentially, leading to the model predictions we observed in which increased activation of

Version of record at: https://doi.org/10.1002/aic.18033



afferents relative to efferents was necessary to reproduce the experimental data.[32,76]

The larger fluctuations in the RR interval predicted by the model are due to species differences. The model represents human RSA, whereas the experimental data are from Yorkshire pigs,[15] which are known to have a lower RSA amplitude.[69] As shown in Figure 6, our model has an RSA amplitude appropriate for humans.

The model makes predictions of the cardiovascular metrics systolic blood pressure, diastolic blood pressure, heart rate, cardiac output, and ejection fraction that match clinical hemodynamic and cardiovascular behavior (Table 2); all cardiovascular metrics are within one standard deviation of reported ranges for healthy women.[34,35] Given that these are emergent features of the model, these data suggest that the model provides an appropriate representation of cardiovascular system dynamics.

We validated further our model's predictions of VNS using a separate experimental data set on VNS in Yorkshire pigs.[32] The experimental cervical VNS stimulus intensity was determined by increasing stimulation until an approximately 10% change in heart rate was achieved. Analogously, we increased stimulation frequency in our model until we achieved a similar heart rate change (Table 2). Using the same stimulation settings as found in Figure 7 (100% afferent stimulation, 50% efferent stimulation), the resulting systolic and diastolic blood pressure changes match the observed experimental changes, indicating that our model is able to predict hemodynamic changes during VNS.

### 3.4 | Modeling opportunities and limitations

Although the model is, to our knowledge, the most comprehensive quantitative model of ICN and brainstem contributions to the control of cardiovascular behavior and RSA, it does not account for all effects that may be of interest. Not explicitly included in the model are the chemoreceptors, which sense blood oxygen and carbon dioxide levels to provide sensory feedback under conditions of hypoxia and hypercapnia.[77] The respiratory feedback information supplied by chemoreceptors contributes to respiratory control, but is also partially captured by the inclusion of lung stretch receptors in the model, except in specific cases such as apnea. Although the omission of chemoreceptors from the model limits the types of conclusions that can be drawn on cardiorespiratory coupling in response to blood gas levels, it provides the opportunity in future work to improve the model so that it can be used to understand cardiovascular and respiratory behavior.

Our model considers the firing rate of the neurons as an important variable that links the neural firing rate to the effects on the end organ. We model the firing rate as a sigmoidal function of the inputs as an approximate accounting of the experimentally observed physiology.[16,59,60] The incorporation of a dynamic model of neurons, for example using detailed ion channel kinetics, is possible and provides an opportunity to build upon the present model.

Furthermore, the implications of ICN dynamics in disease phenotypes such as heart failure and atrial fibrillation, which can arise from autonomic nervous system activation, were not explored.[78] Depending on the disease state, modifications can be made to parameter values or additional equations to represent disease dynamics can be added. In the case of heart failure, stiffening of the left ventricle could be modeled by adjusting the parameters describing left ventricular compliance and resistance. In conjunction with an expansion to model disease states, VNS stimulation parameters could be considered as differentially altering the frequencies of different efferent fiber types and sensory afferent firing rates to represent different scenarios of VNS settings.

## 4 | CONCLUSIONS

We present a new computational model of the closed-loop control of cardiovascular physiology that incorporates detailed anatomical and functional data on central and intrinsic cardiac neural circuits and their interactions with respiration. Our model accounts for and matches experimental observations on RSA as well as VNS effects on heart rate. Our results show that tuning the ICN parameters based on heart rate, elastance, and ICN firing frequency was sufficient to produce a model that represents the approximately linear relationship between the lung tidal volume and the RSA amplitude. This result indicates that the ICN contributes to RSA by maintaining the variations in parasympathetic activity with respiration, providing new insight into the functional role of the ICN beyond serving as a local relay for central reflex control. Furthermore, when we explored our model for multiple scenarios of VNS, we found that a lower relative activation of vagal efferents (motor) compared to vagal afferents (sensory) was necessary to produce physiological behavior consistent with the experimental results. Thus, our results support the notion that VNS activates vagal efferents and afferents differentially, likely in varying proportions depending on the parameters of stimulation. These results inform the emerging studies on exploring and tuning VNS, several of which are supported by the NIH Common Fund SPARC Program.[79,80] Our closed-loop cardiovascular control model is primed for use in such studies aimed at developing bioelectronic interventions to renormalize cardiovascular physiology and treat heart failure.

### 4.1 | Plain language summary

We developed a computational model of the human body's blood pressure regulation system which is mediated by signaling between the brain and the heart. We incorporated into our model contributions of the brainstem, respiratory system as well the neurons surrounding the heart.

#### AUTHOR CONTRIBUTIONS

**Michelle M. Gee:** Data curation (equal); formal analysis (equal); investigation (equal); methodology (equal); software (equal); validation (equal); visualization (equal); writing – original draft (lead); writing – review and editing (supporting). **Abraham M. Lenhoff:** Formal analysis

Version of record at: https://doi.org/10.1002/aic.18033



(supporting); investigation (supporting); methodology (supporting); supervision (supporting); writing – review and editing (supporting). **James S. Schwaber:** Funding acquisition (supporting); investigation (supporting); methodology (supporting); supervision (supporting); writing – review and editing (supporting). **Babatunde A. Ogunnaike:** Conceptualization (equal); formal analysis (supporting); methodology (supporting); project administration (supporting); supervision (supporting). **Rajanikanth Vadigepalli:** Conceptualization (lead); formal analysis (equal); funding acquisition (equal); investigation (equal); methodology (equal); project administration (equal); supervision (lead); visualization (equal); writing – review and editing (equal).

## FUNDING INFORMATION


- U01 HL133360 and R01 HL161696 grants through National Heart, Lung, and Blood Institute.
- National Institutes of Health Common Fund SPARC Program Grant OT2 OD030534.
- National Science Foundation Graduate Research Fellowship Program Grant 1940700.
- Computational resources from the DARWIN computing project at the University of Delaware are made possible by National Science Foundation award OAC-1919839.


## DATA AVAILABILITY STATEMENT

All model files used to generate the figures and the results are available on GitHub (https://github.com/Daniel-Baugh-Institute/CardiovascularControl/tree/main/v03; Version 3, 2022). Data sources used to develop the model are summarized in Table 1.

## ORCID


*Michelle M. Gee* https://orcid.org/0000-0003-4179-5711

*Rajanikanth Vadigepalli* https://orcid.org/0000-0002-8405-1037


## REFERENCES


1. Guyenet PG. The sympathetic control of blood pressure. *Nat Rev Neurosci*. 2006;7(5):335-346.
2. Mortara A, La Rovere MT, Pinna GD, et al. Arterial baroreflex modulation of heart rate in chronic heart failure: clinical and hemodynamic correlates and prognostic implications. *Circulation*. 1997;96(10):3450-3458.
3. Park JH, Gorky J, Ogunnaike B, Vadigepalli R, Schwaber JS. Investigating the effects of brainstem neuronal adaptation on cardiovascular homeostasis. *Front Neurosci*. 2020;14:470.
4. Salavatian S, Beaumont E, Longpré JP, et al. Vagal stimulation targets select populations of intrinsic cardiac neurons to control neurally induced atrial fibrillation. *Am J Physiol Heart Circ Physiol*. 2016;311(5):H1311-H1320.
5. Shinohara T, Shen MJ, Han S, et al. Heart failure decreases nerve activity in the right atrial ganglionated plexus. *J Cardiovasc Electrophysiol*. 2012;23(4):404-412.
6. Achanta S, Gorky J, Leung C, et al. A comprehensive integrated anatomical and molecular atlas of rat intrinsic cardiac nervous system. *iScience*. 2020;23(6):101140.
7. Taylor JA, Eckberg DL. Fundamental relations between short-term RR interval and arterial pressure oscillations in humans. *Circulation*. 1996;93(8):1527-1532.
8. Farmer DGS, Dutschmann M, Paton JFR, Pickering AE, McAllen RM. Brainstem sources of cardiac vagal tone and respiratory sinus arrhythmia. *J Physiol*. 2016;594(24):7249-7265.
9. Vaseghi M, Salavatian S, Rajendran PS, et al. Parasympathetic dysfunction and antiarrhythmic effect of vagal nerve stimulation following myocardial infarction. *JCI. Insight*. 2017;2(16):e86715. doi:10.1172/jci.insight.86715
10. Cheng Z, Powley TL, Schwaber JS, Doyle FJ. Vagal afferent innervation of the atria of the rat heart reconstructed with confocal microscopy. *J Comp Neurol*. 1997;381(1):1-17.
11. Cheng Z, Powley TL, Schwaber JS, Doyle FJ 3rd. Projections of the dorsal motor nucleus of the vagus to cardiac ganglia of rat atria: an anterograde tracing study. *J Comp Neurol*. 1999;410(2):320-341.
12. Armour JA. Potential clinical relevance of the "little brain" on the mammalian heart. *Exp Physiol*. 2008;93(2):165-176.
13. Rajendran PS, Nakamura K, Ajijola OA, et al. Myocardial infarction induces structural and functional remodelling of the intrinsic cardiac nervous system. *J Physiol*. 2016;594(2):321-341.
14. Moss A, Robbins S, Achanta S, et al. A single cell transcriptomics map of paracrine networks in the intrinsic cardiac nervous system. *iScience*. 2021;24(7):102713.
15. Rajendran P, Vaseghi M, Ardell J. Functional recordings from the pig intrinsic cardiac nervous system (ICN). 2019. doi:10.26275/OWRI-MPSX
16. Ursino M. Interaction between carotid baroregulation and the pulsating heart: a mathematical model. *Am J Physiol*. 1998;275(5):H1733-H1747.
17. Ursino M, Magosso E. Short-term autonomic control of the cardiorespiratory system: a summary with the help of a comprehensive mathematical model. *Conf Proc IEEE Eng Med Biol Soc*. 2006;2006:354-358.
18. Rose WC, Rybak IA, Schwaber JS. Closed loop model of vagally-mediated baroreflex control of heart rate. *Conf Proc IEEE Eng Med Biol Soc*. 1995;2:1367–1368.
19. Henson MA, Ogunnaike BA, Schwaber JS, Doyle FJ. The baroreceptor reflex: a biological control system with applications in chemical process control. *Ind Eng Chem Res*. 1994;33(10):2453-2466.
20. Haberbusch M, De Luca D, Moscato F. Changes in resting and exercise hemodynamics early after heart transplantation: a simulation perspective. *Front Physiol*. 2020;11:579449.
21. Vadigepalli R, Doyle FJ 3rd, Schwaber JS. Analysis and neuronal modeling of the nonlinear characteristics of a local cardiac reflex in the rat. *Neural Comput*. 2001;13(10):2239-2271.
22. Park J, Brureau A, Kernan K, et al. Inputs drive cell phenotype variability. *Genome Res*. 2014;24(6):930-941.
23. O'Callaghan EL, Lataro RM, Roloff EL, et al. Enhancing respiratory sinus arrhythmia increases cardiac output in rats with left ventricular dysfunction. *J Physiol*. 2020;598(3):455-471.
24. Shanks J, Abukar Y, Lever NA, et al. Reverse re-modelling chronic heart failure by reinstating heart rate variability. *Basic Res Cardiol*. 2022;117(1):4.
25. Beaumont E, Wright GL, Southerland EM, et al. Vagus nerve stimulation mitigates intrinsic cardiac neuronal remodeling and cardiac hypertrophy induced by chronic pressure overload in Guinea pig. *Am J Physiol Heart Circ Physiol*. 2016;310(10):H1349-H1359.
26. Shinlapawittayatorn K, Chinda K, Palee S, et al. Low-amplitude, left vagus nerve stimulation significantly attenuates ventricular dysfunction and infarct size through prevention of mitochondrial dysfunction during acute ischemia-reperfusion injury. *Heart Rhythm*. 2013;10(11):1700-1707. doi:10.1016/j.hrthm.2013.08.009
27. De Ferrari GM, Stolen C, Tuinenburg AE, et al. Long-term vagal stimulation for heart failure: eighteen month results from the NEural Cardiac TherApy foR Heart Failure (NECTAR-HF) trial. *Int J Cardiol*. 2017;244:229-234.
28. Premchand RK, Sharma K, Mittal S, et al. Autonomic regulation therapy via left or right cervical vagus nerve stimulation in patients with chronic heart failure: results of the ANTHEM-HF trial. *J Card Fail*. 2014;20(11):808-816.

Version of record at: https://doi.org/10.1002/aic.18033



29. Stavrakis S, Humphrey MB, Scherlag BJ, et al. Low-level transcutaneous electrical vagus nerve stimulation suppresses atrial fibrillation. *J Am Coll Cardiol*. 2015;65(9):867-875.
30. Iano TL, Levy MN, Lee MH. An acceleratory component of the parasympathetic control of heart rate. *Am J Physiol*. 1973;224(5):997-1005.
31. Falkenburger BH, Jensen JB, Hille B. Kinetics of M1 muscarinic receptor and G protein signaling to phospholipase C in living cells. *J Gen Physiol*. 2010;135(2):81-97.
32. Yamakawa K, So EL, Rajendran PS, et al. Electrophysiological effects of right and left vagal nerve stimulation on the ventricular myocardium. *Am J Physiol Heart Circ Physiol*. 2014;307(5):H722-H731.
33. Kobayashi H. Normalization of respiratory sinus arrhythmia by factoring in tidal volume. *Appl Human Sci*. 1998;17(5):207-213.
34. Teixeira AL, Fernandes W, Moraes EM, Alves H, Damasceno VO, Dias MR. Effects of menstrual cycle phase on resting heart rate in healthy women. *J Exerc Physiol Online*. 2012;15(4):47-54.
35. Cain PA, Ahl R, Hedstrom E, et al. Age and gender specific normal values of left ventricular mass, volume and function for gradient echo magnetic resonance imaging: a cross sectional study. *BMC Med Imaging*. 2009;9:2.
36. Magosso E, Ursino M. A mathematical model of $CO_2$ effect on cardiovascular regulation. *Am J Physiol Heart Circ Physiol*. 2001;281(5):H2036-H2052.
37. Ursino M, Magosso E. Acute cardiovascular response to isocapnic hypoxia. I. A mathematical model. *Am J Physiol Heart Circ Physiol*. 2000;279(1):H149-H165.
38. Magosso E, Cavalcanti S, Ursino M. Theoretical analysis of rest and exercise hemodynamics in patients with total cavopulmonary connection. *Am J Physiol Heart Circulat Physiol*. 2002;282(3):H1018-H1034. doi:10.1152/ajpheart.00231.2001
39. Ursino M, Magosso E. Interaction among humoral and neurogenic mechanisms in ventilation control during exercise. *Ann Biomed Eng*. 2004;32(9):1286-1299.
40. Mendelowitz D. Advances in parasympathetic control of heart rate and cardiac function. *News Physiol Sci*. 1999;14:155-161.
41. Lopes OU, Palmer JF. Proposed respiratory "gating" mechanism for cardiac slowing. *Nature*. 1976;264(5585):454-456.
42. Eckberg DL. The human respiratory gate. *J Physiol*. 2003;548(2):339-352.
43. Taylor EW, Leite CAC, Sartori MR, Wang T, Abe AS, Crossley DA 2nd. The phylogeny and ontogeny of autonomic control of the heart and cardiorespiratory interactions in vertebrates. *J Exp Biol*. 2014;217(Pt 5):690-703.
44. Dergacheva O, Griffioen KJ, Neff RA, Mendelowitz D. Respiratory modulation of premotor cardiac vagal neurons in the brainstem. *Respir Physiol Neurobiol* 2010;174(1–2):102–110.
45. Ben-Tal A, Shamailov SS, Paton JFR. Central regulation of heart rate and the appearance of respiratory sinus arrhythmia: new insights from mathematical modeling. *Math Biosci*. 2014;255:71-82.
46. Hadaya J, Ardell JL. Autonomic modulation for cardiovascular disease. *Front Physiol*. 2020;11:617459.
47. Fedele L, Brand T. The intrinsic cardiac nervous system and its role in cardiac pacemaking and conduction. *J Cardiovasc Dev Dis*. 2020;7(4):54. doi:10.3390/jcdd7040054
48. Cheng Z, Zhang H, Guo SZ, Wurster R, Gozal D. Differential control over postganglionic neurons in rat cardiac ganglia by NA and DmnX neurons: anatomical evidence. *Am J Physiol Regul Integr Comp Physiol*. 2004;286(4):R625-R633.
49. Cheng Z, Powley TL. Nucleus ambiguus projections to cardiac ganglia of rat atria: an anterograde tracing study. *J Comp Neurol*. 2000;424(4):588-606.
50. Mastitskaya S, Marina N, Gourine A, et al. Cardioprotection evoked by remote ischaemic preconditioning is critically dependent on the activity of vagal pre-ganglionic neurones. *Cardiovasc Res*. 2012;95(4):487-494.
51. Machhada A, Ang R, Ackland GL, et al. Control of ventricular excitability by neurons of the dorsal motor nucleus of the vagus nerve. *Heart Rhythm*. 2015;12(11):2285-2293.
52. Machhada A, Marina N, Korsak A, Stuckey DJ, Lythgoe MF, Gourine AV. Origins of the vagal drive controlling left ventricular contractility. *J Physiol*. 2016;594(14):4017-4030.
53. Jones JF, Wang Y, Jordan D. Activity of C fibre cardiac vagal efferents in anaesthetized cats and rats. *J Physiol*. 1998;507(Pt 3):869-880.
54. Wang J, Irnaten M, Neff RA, et al. Synaptic and neurotransmitter activation of cardiac vagal neurons in the nucleus ambiguus. *Ann NY Acad Sci*. 2001;940:237-246.
55. Ardell JL, Armour JA. Neurocardiology: structure-based function. *Compr Physiol*. 2016;6(4):1635-1653.
56. Del Rio R, Marcus NJ, Schultz HD. Carotid chemoreceptor ablation improves survival in heart failure: rescuing autonomic control of cardiorespiratory function. *J Am Coll Cardiol*. 2013;62(25):2422-2430.
57. Niewinski P. Carotid body modulation in systolic heart failure from the clinical perspective. *J Physiol*. 2017;595(1):53-61.
58. Paton JFR, Sobotka PA, Fudim M, et al. The carotid body as a therapeutic target for the treatment of sympathetically mediated diseases. *Hypertension*. 2013;61(1):5-13.
59. Rogers RF, Paton JF, Schwaber JS. NTS neuronal responses to arterial pressure and pressure changes in the rat. *Am J Physiol*. 1993;265(6 Pt 2):R1355-R1368.
60. Kawada T, Sugimachi M, Shishido T, et al. Simultaneous identification of static and dynamic vagosympathetic interactions in regulating heart rate. *Am J Physiol*. 1999;276(3):R782-R789.
61. Levy MN, Iano T, Zieske H. Effects of repetitive bursts of vagal activity on heart rate. *Circ Res*. 1972;30(2):186-195.
62. Pianosi F, Wagener T. Distribution-based sensitivity analysis from a generic input-output sample. *Environ Model Software*. 2018;108:197-207.
63. Bratley P, Fox BL. Algorithm 659: implementing Sobol's quasirandom sequence generator. *ACM Trans Math Softw*. 1988;14(1):88-100.
64. Hong HS, Hickernell FJ. Algorithm 823: implementing scrambled digital sequences. *ACM Trans Math Softw*. 2003;29(2):95-109.
65. Joe S, Kuo FY. Remark on algorithm 659: implementing Sobol's quasirandom sequence generator. *ACM Trans Math Softw*. 2003;29(1):49-57.
66. Yang CF, Yu-Chih Chen M, Chen TI, Cheng CF. Dose-dependent effects of isoflurane on cardiovascular function in rats. *Tzu Chi Med J*. 2014;26(3):119-122.
67. Scholkopf B, Peters J, Janzing D. *Elements of Causal Inference: Foundations and Learning Algorithms*. MIT Press; 2017.
68. Sundaramoorthy AS, Varanasi SK, Huang B, Ma Y, Zhang H, Wang D. Sparse inverse covariance estimation for causal inference in process data analytics. *IEEE Trans Control Syst Technol*. 2022;30(3):1268-1280.
69. Detweiler DK. The mammalian electrocardiogram: comparative features. In: Macfarlane PW, van Oosterom A, Pahlm O, Kligfield P, Janse M, Camm J, eds. *Comprehensive Electrocardiology*. Springer; 2010.
70. Erdemir A, Mulugeta L, Ku JP, et al. Credible practice of modeling and simulation in healthcare: ten rules from a multidisciplinary perspective. *J Transl Med*. 2020;18(1):369.
71. Ben-Tal A, Shamailov SS, Paton JFR. Evaluating the physiological significance of respiratory sinus arrhythmia: looking beyond ventilation-perfusion efficiency: respiratory sinus arrhythmia function. *J Physiol*. 2012;590(8):1989-2008.
72. Prechtl JC, Powley TL. The fiber composition of the abdominal vagus of the rat. *Anat Embryol*. 1990;181(2):101-115.
73. Pečlin P, Rozman J. Alternative paradigm of selective vagus nerve stimulation tested on an isolated porcine vagus nerve. *Sci World J*. 2014;2014:310283.
74. Gorman PH, Mortimer JT. The effect of stimulus parameters on the recruitment characteristics of direct nerve stimulation. *IEEE Trans Biomed Eng*. 1983;30(7):407-414.

Version of record at: https://doi.org/10.1002/aic.18033



75. Ahmed U, Chang YC, Cracchiolo M, et al. Anodal block permits directional vagus nerve stimulation. *Sci Rep*. 2020;10(1):9221.
76. Ardell JL, Nier H, Hammer M, et al. Defining the neural fulcrum for chronic vagus nerve stimulation: implications for integrated cardiac control. *J Physiol*. 2017;595(22):6887-6903.
77. Kara T, Narkiewicz K, Somers VK. Chemoreflexes—physiology and clinical implications. *Acta Physiol Scand*. 2003;177(3):377-384.
78. Chen PS, Chen LS, Fishbein MC, Lin SF, Nattel S. Role of the autonomic nervous system in atrial fibrillation: pathophysiology and therapy. *Circ Res*. 2014;114(9):1500-1515.
79. SPARC Portal. Accessed October 26, 2022. https://sparc.science/
80. Neuromod Prize. Accessed October 26, 2022. https://www.neuromodprize.com/

## SUPPORTING INFORMATION

Additional supporting information can be found online in the Supporting Information section at the end of this article.

**How to cite this article:** Gee MM, Lenhoff AM, Schwaber JS, Ogunnaike BA, Vadigepalli R. Closed-loop modeling of central and intrinsic cardiac nervous system circuits underlying cardiovascular control. *AIChE J*. 2023;69(4):e18033. doi:10.1002/aic.18033